

TO: Distribution
DATE: September 29, 1982

FROM: Hans Keppler *kep*
MAIL STOP/TELEPHONE: J981/7-4318

SYMBOL: ESS-4-82-1

SUBJECT: THREE HYPOTHESES ON THE PRINCIPAL STRESS
DIRECTIONS IN THE FENTON HILL PHASE II RESERVOIR

Summary

We owe new information on the state of stress around the EE-2 and EE-3 openhole sections to Fred Homuth and Dan Cash: a preliminary fault-plane solution of earthquakes triggered after our June 04, 1982 pumping shows clear evidence of a strike slip mechanism. This does not match any of the previous conceptions of the subsurface stress field.

Directions of principal stresses as inferred from Phase I - Observations.

During fracturing operations in the Phase I reservoir the located microearthquakes distributed about nearly vertical planar zones striking consistently around N160 E. Examples are the experiments 203 and 195 (Figure 1a) and the "Stress Unlocking Experiment" (compare e.g. ALBRIGHT & PEARSON, 1980, MURPHY, et al, 1981, DASH, et al 1981). This observation, together with the predominantly high s - to - p - wave amplitude ratio, was unanimously interpreted as hydraulic, or tensile, fractures accompanied by shear failure or slippage induced by the pore pressure increase away from their surfaces. (HDR-STAFF, 1980, PEARSON, 1981). The pertinent direction of the least principal stress, σ_3 , is then horizontal and roughly N70 E as indicated by AB in Figure 1a. Together with the belief, that the overburden yields the maximum principal stress, σ_1 the stress field displayed in Figure 1b results. The dashed lines represent the most likely directions for shear motion: a normal faulting mechanism.

Microearthquakes occurring on either one of such planes would result in a fault-plane solution as shown in Figure 1c. (Stereographic or equal angle projection to the upper hemisphere of the focal sphere, the dark sections representing compressional first motions, P is the compression or σ_3 axis). Based on this philosophy on the stress field, the wellbores EE-2 and EE-3 have been drilled in the present direction.

Phase II Fracture Pattern

First realized in Experiment 2007 (second pressurization test of EE-3) we located the origin of microearthquakes throughout our 1982 spring-summer fracturing attempts on inclined oblate zones striking very similar to the Phase I seismic distributions and dipping between 15° and 60° towards west (thus defining flat regions roughly perpendicular to the wellbores). Without further detailing how much of the spread of the locations on these features may be due to errors of our one tool hodogram method, I would consent to the belief that we did deal with lateral distributions. Figure 2a gives a typical example of such a hypocentral distribution. This observation suggested again that hydraulically created or tensile fractures yielded a duct to regions where the pore pressure was increased and thus shear events were triggered. The additional observation of a cloud-like spread of the origins as pumping went on seemed to confirm this philosophy.

The pertinent stress field is shown in Figure 2b and the fault-plane solution in Figure 2c represents the consistent radiation pattern for this model implying a near dip slip motion or normal faulting on a very gentle slope. Bill Laughlin (1982) pointed out, that this hypothesis can plausibly be explained by the tectonics of a near-by subsiding magma reservoir (Figure 2d).

Radiation Pattern Observed After the June 04 Pumping Experiment (2012)

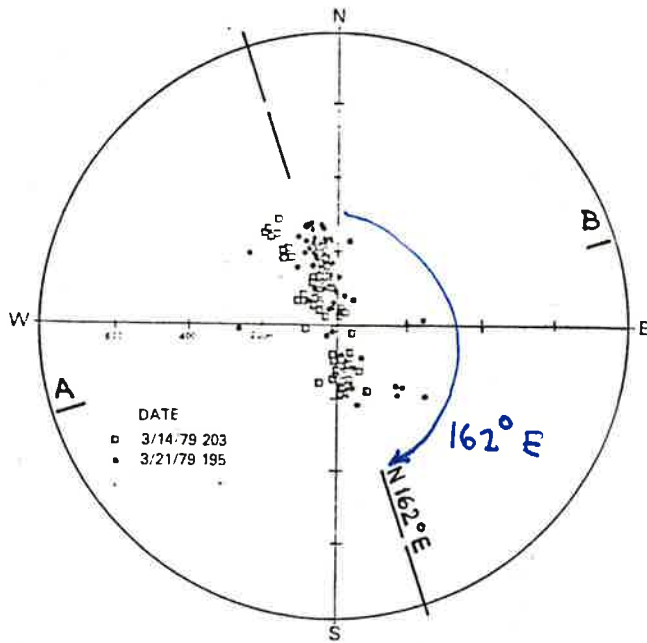
Alerted by the relatively large magnitudes of microearthquakes triggered during the first pump (May 30, Experiment 2011), Fred Homuth put up a close in net of ESS-3 seismic field stations with high quality recording (telemetric and magn. tape recording) furnishing both proof of the relation of the hypocenters to the fracturing operation and the capability of resolving the radiation patterns of the stronger quakes.

During June 05, 16 earthquakes could be recorded with consistent first motions on all of the 14 stations. Dan Cash's fault-plane solution is shown in Figure 3. Note that the uncertain first motions arrange close to the nodal planes confirming the pertinent radiation pattern. Differing widely from the expected cases in Figures 1c and 2c, the solution shows a left lateral strike slip on a $N2.5^\circ(\pm 1.5^\circ)E$ striking and $73^\circ(\pm 1^\circ)$ dipping plane or a right lateral strike slip on a $N94^\circ(\pm 2^\circ)E$ striking and $86.5^\circ(\pm 6.5^\circ)$ dipping plane. Hence the planes of motion are unusually well-defined, only when one or the other uncertain point is included in the "wrong" quadrant, the tolerance becomes, of course, greater (as demonstrated in Figure 4b with BACB). The present solution did not apply corrections for geologically realistic velocity models in calculating the take-off angles. However such corrections would noticeably only effect the stations further away from the epicenter and shift e.g. the points for rEDP or JEPT a few degrees away from the center. This would hardly - if at all - change the nodal planes (mainly because it refers to a strike slip solution). The existence of compressive and dilational quadrants in the p-wave radiation pattern also proves (for the first time directly) that our source mechanism is a shear mode.

The directions of the principal stresses are usually derived from fault-plane solutions assuming that the fault plane is a plane of maximum shear. These directions are displayed in Figures 3 and 4; the T-axis denotes the σ_3 - direction and the P-axis defines the σ_1 - direction. However if the fault plane of the observed earthquakes is a reactivated tectonic feature from Fenton Hill's geological past rather than a plane of maximum shear stress, the compressive axis (P or σ_1) does not necessarily have to be located in the center of the dilational quadrant, but it is still restricted to lie within the dilational quadrant on the focal sphere (AKI & RICHARDS, 1980, MCKENZIE, 1969). As can be seen from a comparison of Figure 4a with 1c or 2c, the obtained fault-plane solution is sufficiently different from the former conceptions to be inconsistent even under this broad-minded assumption.

Conclusions

1. We have to drop at least two of the above made assumptions in order to attain a consistent idea of the orientation of the Fenton Hill subsurface stress field, e.g. assume in future that our hydraulic ducts are

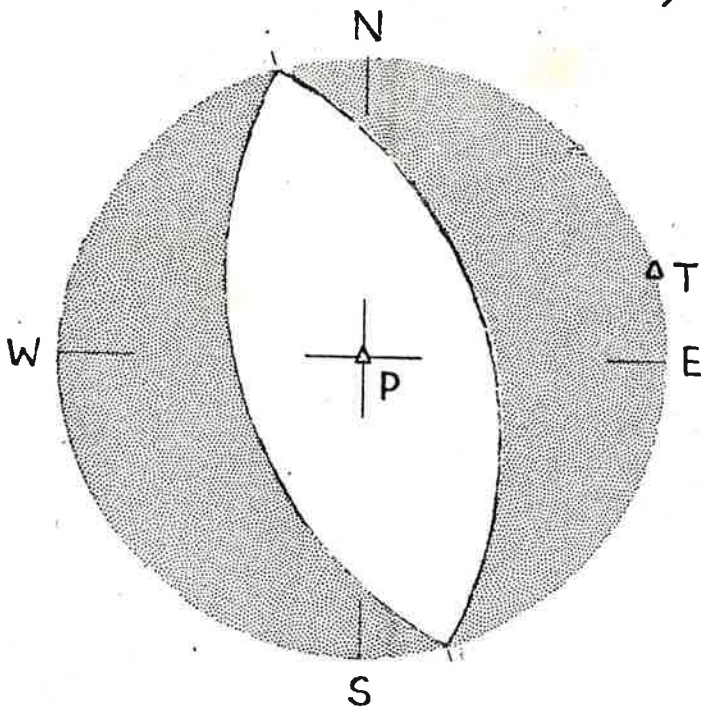
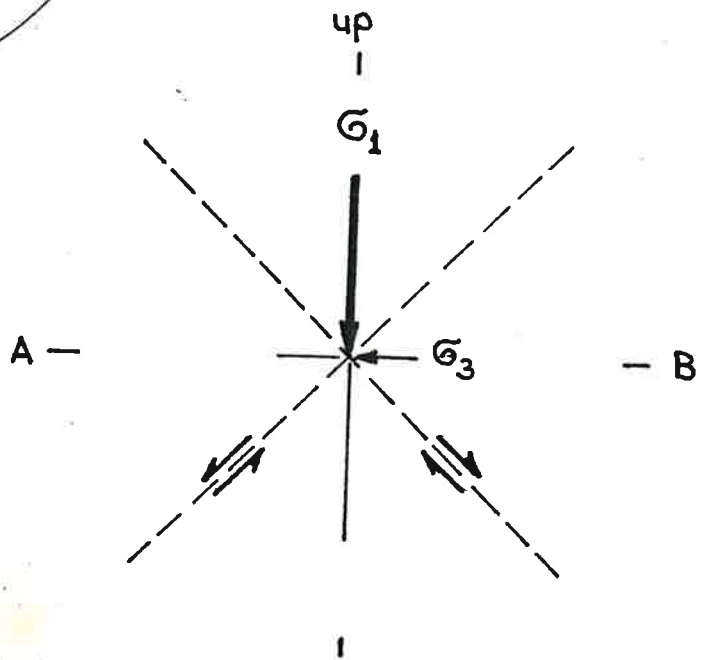


a

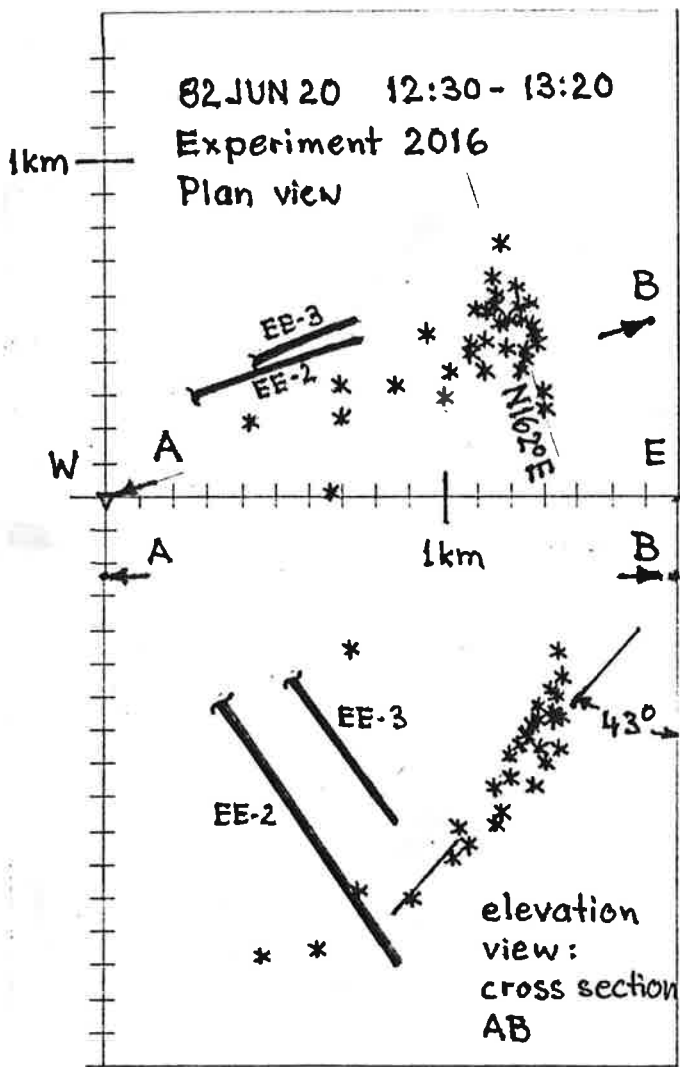
Figure 1.

- a) Examples for the Distribution of Seismicity in the Phase I Reservoir.
- b) Pertinent Stress Directions and
- c) Fault-plane solution

b

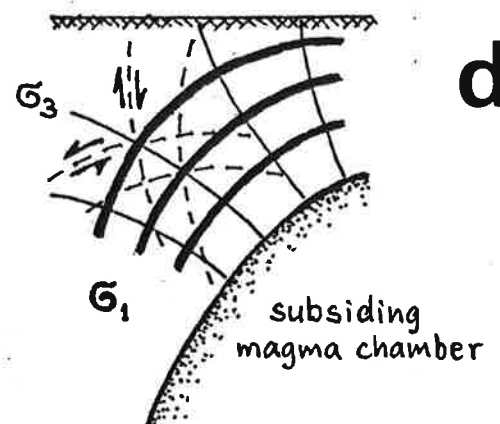
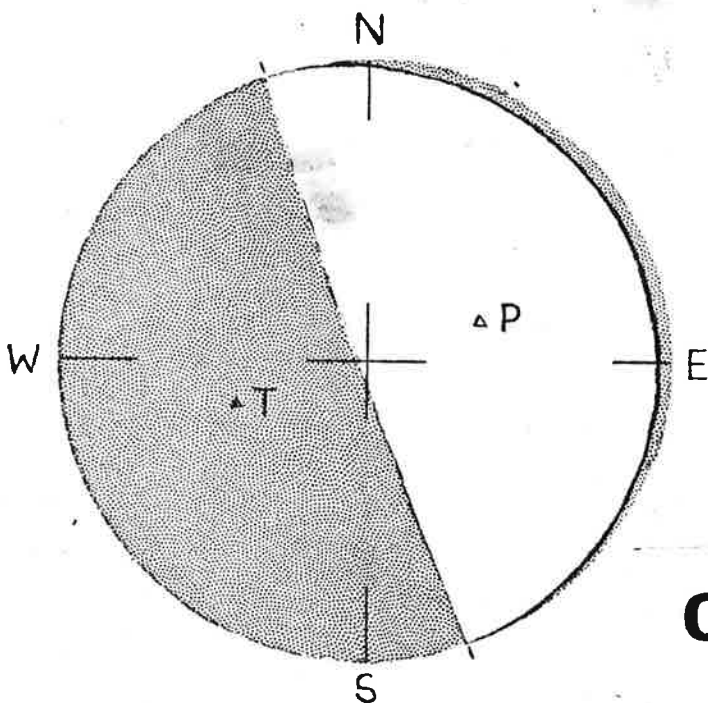
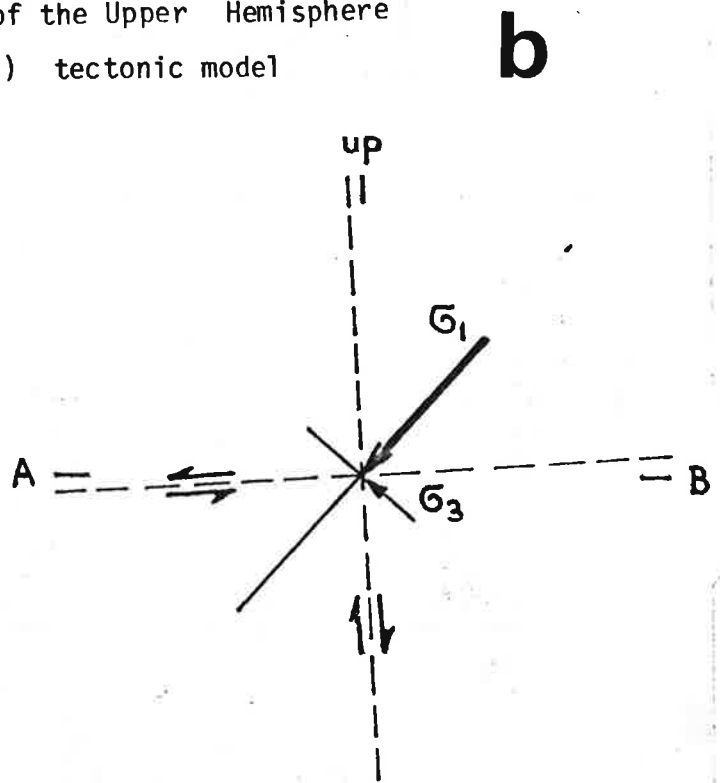


c



a Figure 2.

- a) Examples for the Distribution of Micro-earthquake Foci During a Phase II Fracturing Attempt
 b) Pertinent Stress Field
 c) Fault-plane Solution (stereographic Projection of the Upper Hemisphere)
 d) tectonic model



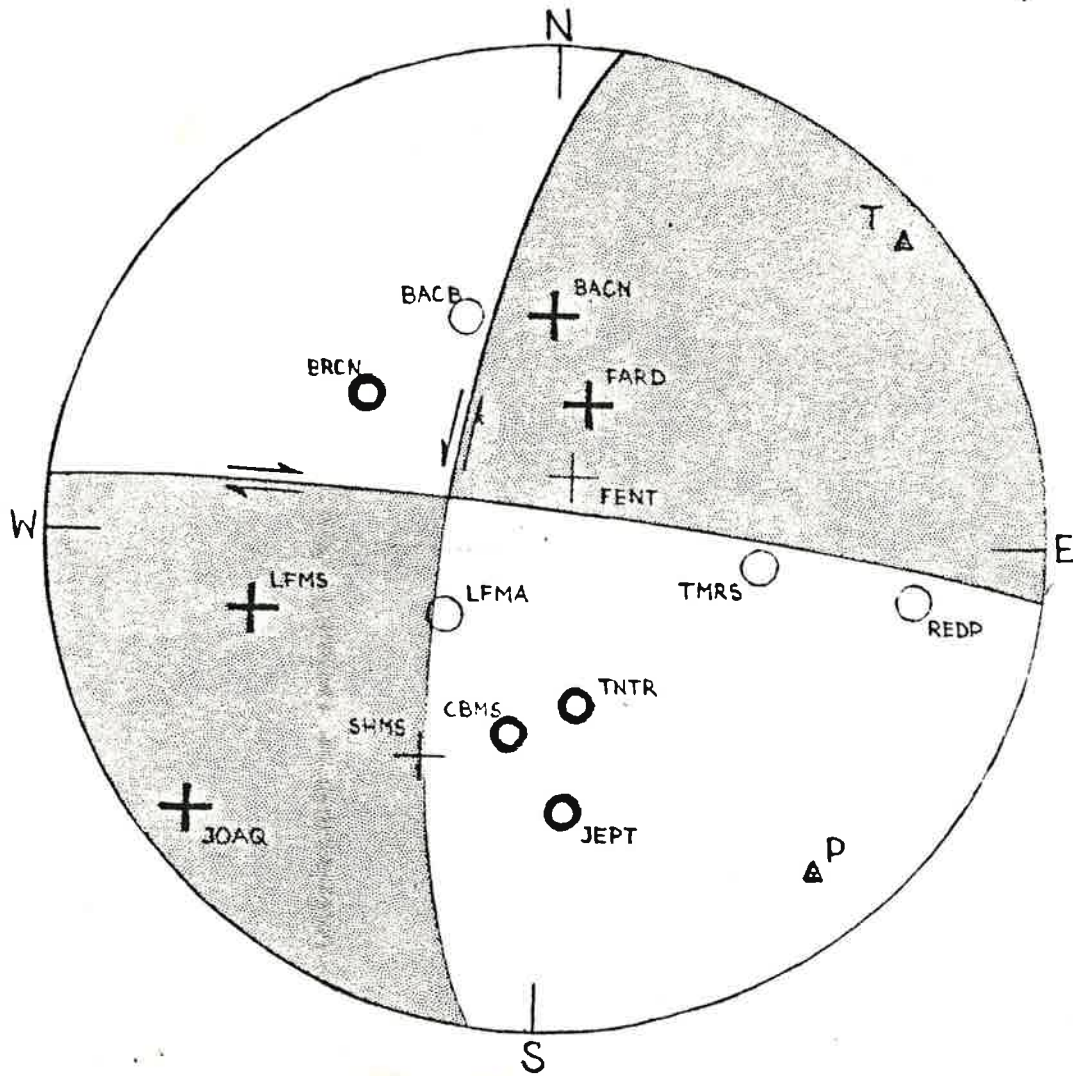
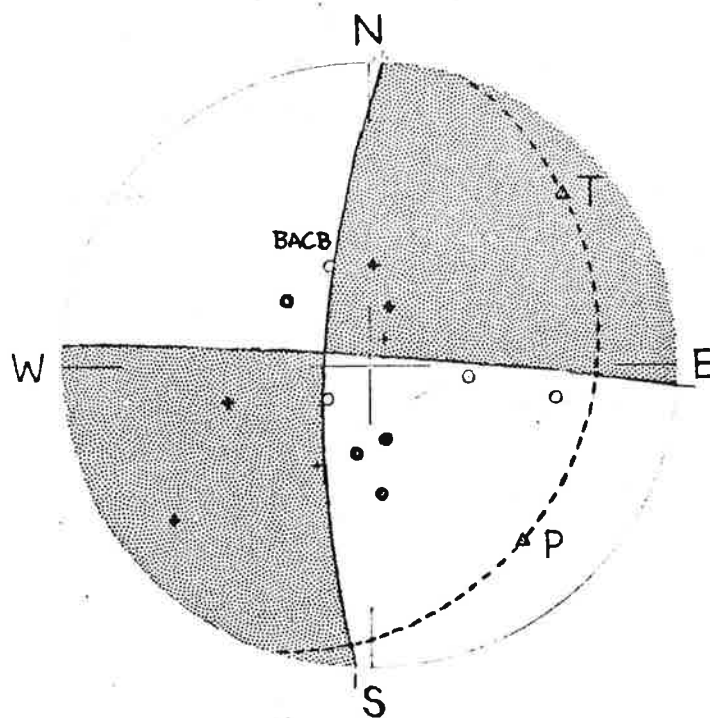
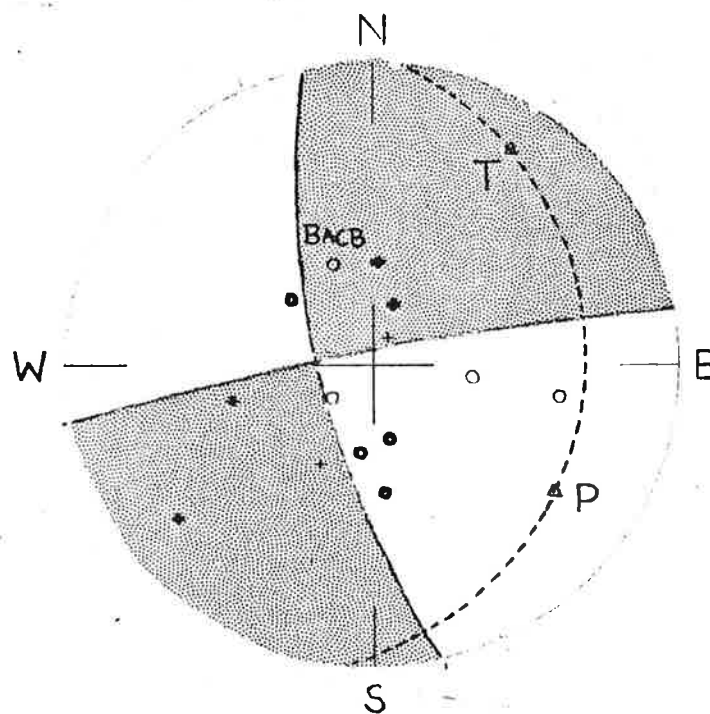


Figure 3. Zenithal Equal-Area Projection of the Upper Hemisphere of the Focal Sphere for 16 Microearthquakes Recorded After Experiment 2012 (82 JUN 05) With the Local ESS-3 Net. Crosses Denote compressions, Circles Dilatations. Fat Symbols mean High Confidence in Determined First Motion, Lean Faced Ones Represent Stations with Weak p-Arrivals.



a



b

Figure 4. a) Stereographic (equal-angle) Projection of the Fault Plane solution of Figure 3. b) Example for Possible Changes of the Fault-Planes if a Station With Doubtful First Motion is Moved Across the Nodal Plane.